JACS
JOURNAL OF THE AMERICAN CHEMICAL SOCIETY
Article
Cite This: J. Am. Chem. Soc. 2018, 140, 7885−7895
pubs.acs.org/JACS

Gating Mechanism of Aquaporin Z in Synthetic Bilayers and Native Membranes Revealed by Solid-State NMR Spectroscopy

Yongxiang Zhao,[†,▽,⊗] Huayong Xie,[†,▽,⊗] Lili Wang,[‡,§] Yang Shen,[#] Wei Chen,[†,▽] Benteng Song,[†] Zhengfeng Zhang,[†] Anmin Zheng,[†] Qingsong Lin,[‡,§] Riqiang Fu,[⊥] Jufang Wang,[*,∥] and Jun Yang[*,†]

[†]National Center for Magnetic Resonance in Wuhan, Key Laboratory of Magnetic Resonance in Biological Systems, State Key Laboratory of Magnetic Resonance and Atomic and Molecular Physics, Wuhan Institute of Physics and Mathematics, Chinese Academy of Sciences, Wuhan 430071, P.R. China

[‡]NUS Environmental Research Institute, National University of Singapore, 117411 Singapore

[§]Department of Biological Sciences, National University of Singapore, 117411 Singapore

[∥]School of Biology and Biological Engineering, South China University of Technology, Guangzhou 510006, P.R. China

[⊥]National High Magnetic Field Laboratory, Tallahassee, Florida 32310, United States

[#]Laboratory of Chemical Physics, National Institute of Diabetes and Digestive and Kidney Diseases, National Institutes of Health, Bethesda, Maryland 20892-0520, United States

[▽]University of Chinese Academy of Sciences, Beijing 100049, P.R. China

Supporting Information

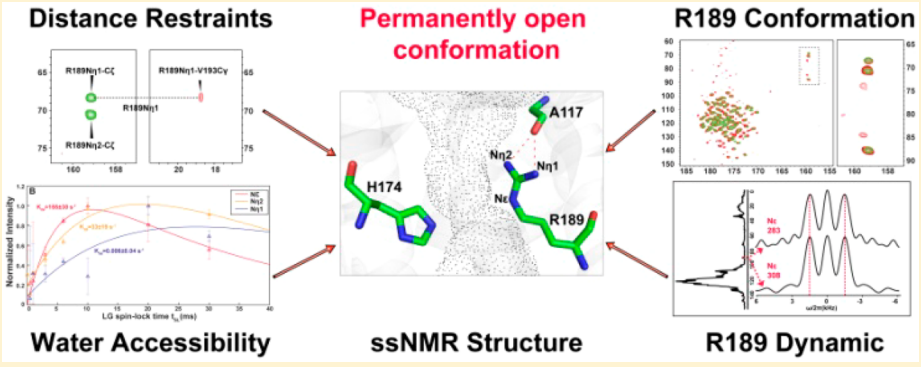

ABSTRACT: Aquaporin Z (AqpZ) is an integral membrane protein that facilitates transport of water across *Escherichia coli* cells with a high rate. Previously, R189, a highly conserved residue of the selective filter of AqpZ, was proposed as a gate within the water channel on the basis of the observation of both open and closed conformations of its side chain in different monomers of an X-ray structure, and the observation of rapid switches between the two conformations in molecular dynamic simulations. However, the gating mechanism of the R189 side chain remains controversial since it is unclear whether the different conformations observed in the X-ray structure is due to different functional states or is a result of perturbation of non-native detergent environments. Herein, in native-like synthetic bilayers and native *E. coli* membranes, a number of solid-state NMR techniques are employed to examine gating mechanism of the R189 side chain of AqpZ. One R189 side-chain conformation is highly evident since only a set of peaks corresponding to the R189 side chain is observed in 2D $^{15}N-^{13}C$ spectra. The immobility of the R189 side chain is detected by $^{1}H-^{15}N$ dipolar lineshapes, excluding the possibility of the rapid switches between the two side-chain conformations. High-resolution monomeric structure of AqpZ, determined by CS-Rosetta calculations using experimentally measured distance restraints related to the R189 side chain, reveals that this side chain is in an open conformation, which is further verified by its water accessibility. All the solid-state NMR experimental results, combining with water permeability essay, suggest a permanently open conformation of the R189 side chain in the synthetic bilayer and native membranes. This study provides new structural insights into the gating mechanism of aquaporins and highlights the significance of lipid bilayer environments in elucidating the molecular mechanism of membrane proteins.

INTRODUCTION

Structures and functions of membrane proteins can be influenced by membrane mimetic environments. 3D structure determination of membrane proteins in native lipid bilayers is

Received: March 29, 2018
Published: May 25, 2018

DOI: 10.1021/jacs.8b03446
J. Am. Chem. Soc. 2018, 140, 7885−7895

still a great challenge, though significant advances have been made for cryo-EM and X-ray crystallography in structure determination of membrane proteins in lipid environments such as liposomes, lipid nanodiscs and lipid cubic phases in the recent years. At present most of membrane protein structures in the Protein Data Bank (PDB) were determined by X-ray crystallography and solution NMR in detergent environments. Despite that many of these structures have native-like properties, perturbations of non-native mimetic environments to the structures have been reported.[1] In the non-native mimetic environments, less hydrophobic thickness, detergent penetration and crystal packing contacts in detergent-based crystals can perturb the native structure of membrane proteins.[2] If the structural perturbations were interpreted as functional states of the protein, it would lead to misinterpretation of the molecular mechanisms. Therefore, structure analysis of membrane proteins in native membranes or native-like lipid bilayers is critical to validate the molecular mechanisms elucidated in the detergent environments. However, the related studies are scarce because of difficulties in structural characterization of membrane proteins in lipid bilayers.

Aquaporins (AQPs) are integral membrane proteins that facilitate movement of water and small, uncharged molecules across cells with a high rate.[3,4] Water permeation, substrate selectivity and gating are three major aspects of the molecular mechanism of AQPs. The understandings of water permeation and substrate selectivity have been advanced by a number of atomic-resolution structures and computer simulations, while the gating mechanism of AQPs[5,6] remains controversial since the gating mechanism was induced indirectly on the basis of a combination of X-ray structures and MD simulations, rather than direct monitoring of the opening and closing of the water channel by electrophysiological techniques. So far two pictures of gating, namely "capping" and "pinching", have emerged.[6] The "capping" mechanism is involved in a large-scale rearrangement of loop residues for capping and opening the water channel. The "pinching" mechanism, which was proposed on the basis of the observation of the small structural variation of a few residues or even a single residue to pinch in upon the ar/R constriction region in X-ray structures, is debatable because it is difficult to identify whether such small structural variation in X-ray structures is attributed to different functional states or structural perturbations of non-native detergent environments.

As an example of "pinching" mechanism, the gating of *Escherichia coli* (*E. coli*) aquaporin Z (AqpZ) remains a controversial issue. Like other AQPs, AqpZ is a tetramer natively and each monomer functions as an independent water channel with an Asn-Pro-Ala (NPA) signature motif and a conserved aromatic/arginine (ar/R) selectivity filter (SF) region.[7,8] Arg-189 (R189), a highly conserved component of the ar/R SF, has been proposed as a gate on the basis of an X-ray structure of AqpZ[9] and molecular dynamic (MD) simulations.[10,11] In the X-ray structure of an asymmetric crystal of AqpZ, all channel-lining residues were found almost identical in four monomeric channels except R189, whose side chains appeared to have distinct conformations in different monomers. In one of the four monomers (A), the guanidino group of R189 adopts an orientation up toward the extracellular side and the water channel is open, while in the remaining three monomers (B, C, D), the guanidino groups of R189 adopt an orientation down toward the water channel, resulting in the closing of the channel.[9] MD simulations revealed rapid flips between the open and closed conformations on the nanosecond time scale.[10,11] However, the gating mechanism of the R189 side chain relies on the observation of distinct conformational states of the R189 side chain in the detergent environments. To investigate whether these distinct conformations are due to a perturbation of non-native detergent environments or resulted from different functional states, it is necessary to examine the mechanism in native membranes or native-like lipid bilayer environments.

Magic angle spinning (MAS) solid-state NMR (ssNMR) has emerged as a powerful technique to elucidate the molecular mechanism of membrane proteins in lipid bilayers.[12−21] Chemical shift is very sensitive to the local chemical environments and can be used to probe subtle conformational states of proteins. In addition, ssNMR has a number of techniques capable of detecting dynamics of proteins on time scales from picoseconds to seconds.[22] In particular, motional-averaged dipolar line-shape is a unique probe for large-amplitude fast motions.[23,24] Furthermore, high-resolution 3D structure of membrane proteins can be determined by ssNMR in native-like lipid bilayers, as demonstrated by several recent studies.[25−28] Herein, we employed a number of ssNMR experiments to investigate the gating mechanism and revealed that the R189 side chain is in a permanently open conformation rather than a gate of the channel of AqpZ. In our study, two lipid environments, synthetic POPC/POPG proteoliposomes and native *E. coli* membranes, were used to examine the gating mechanism of the R189 side chain. In both environments, one stable conformation of the R189 side chain was observed, as evidenced by the presence of one set of corresponding peaks from the R189 side chain in $^{15}N-^{13}C$ correlation spectra. The immobility of the R189 side chain was detected by dipolar lineshapes of $^{1}H-^{15}N_{\varepsilon}$ extracted from dipolar chemical shift correlation (DIPSHFT) experiments in synthetic lipids and native membranes. 3D structure of monomeric AqpZ, which was determined by CS-Rosetta calculations using experimentally measured distance restraints related to the R189 side chain, suggested that the R189 side chain is in an open conformation. The open conformation of the R189 side chain was verified by its water accessibility. This study provided new structural insights into the gating of AQPs and highlighted the importance of native or native-like lipid bilayers environment in elucidating mechanisms of membrane proteins.

EXPERIMENTS AND METHODS

Δ4-AqpZ Mutant Construction, Protein Expression, and Purification. The Δ4-AqpZ (R3K, R75K, R224K, R230K) mutant was constructed by site-directed-mutagenesis of wild-type (wt) pET H6-AqpZ plasmid. The expression vector pET H6-AqpZ encodes full-length *E. coli aqpz* gene (GenBank ID U38664.1) with an N-terminal 6×His tag sequence of MGSSHHHHHHEF.[29] The wt- and Δ4-AqpZ plasmids were expressed in *E. coli* BL21 (DE3) strain by a modified "dual media" approach.[30] Briefly, several expression colonies were inoculated into 100 mL of LB medium with 100 μg/mL ampicillin for cultivation expansion overnight. Next, 10 mL of *E. coli* cell suspension was transferred into 1 L of LB medium, and the cells were harvested by centrifugation at 6000*g* for 10 min until OD_{600} reached 0.6−0.8. After the cells were recovered in 250 mL of M9 medium (4 g/L ^{13}C glucose, 1 g/L ^{15}N NH_4Cl) by shaking in 220 rpm at 310 K for 30 min, 1 mM isopropyl β-D-1-thiogalactopyranoside (IPTG) was added to induce expression at 310 K for 5 h.

To purify AqpZ, the cells were lysed by ultrasonication, and the unbroken cells were removed by low-speed centrifugation at 6000*g* for 10 min. The total cell membranes were collected by high-speed centrifugation at 48384*g* for 1 h and then solubilized into 1% sodium *N*-lauroylsarcosinate at 277 K overnight. The purification was carried

DOI: 10.1021/jacs.8b03446
J. Am. Chem. Soc. 2018, 140, 7885−7895

out using a nickel affinity chromatography. The yield of the expression by the "dual media" approach was 36−44 mg of pure AqpZ per liter of M9 medium culture.

Sample Preparations for ssNMR Experiments. *Proteoliposome Samples.* The wt- or Δ4-AqpZ was reconstituted in 1-palmitoyl-2-oleoyl-*sn*-glycero-3-phosphocholine (POPC)/1-palmitoyl-2-oleoyl-*sn*-glycero-3-[phospho-*rac*-(1-glycerol)] (POPG) liposomes by dialysis. First, the 10 mg/mL POPC/POPG liposome stocks were prepared by hydration and ultrasonic bath methods. Then, the POPC/POPG lipids were dissolved in 2% *n*-dodecylphosphocholine (DPC) and mixed with desired amount AqpZ in 0.5% DPC such that the protein−lipid weight ratio was 1:1.25(w/w). After incubated at 291 K for 2 h, the protein, detergent, and lipid mixture was transferred into 8 kDa dialysis bag against 250× dialysis buffer (20 mM Tris, pH 8.0, 50 mM NaCl) at 291 K. The dialysis buffer was changed every 24 h. After 7 days of dialysis, the proteoliposomes were collected by high-speed centrifugation at 548352*g* for 2 h. The vesicular morphology of the proteoliposomes was checked by negatively stained electron micrographs, as shown in Figure S1 in the Supporting Information. The proteoliposome pellets were freeze-dried for dehydration so that ∼35 mg of U-^{13}C,^{15}N AqpZ or Δ4-AqpZ in proteoliposomes with 30% (w/w) water was packed into thin-wall rotors for ssNMR experiments.

E. coli Inner Membrane Samples. The *E. coli* inner membrane samples with expressed AqpZ were prepared as follows. After expression, the cells were broken, and the total cellular membrane fraction was prepared by differential centrifugation as mentioned above. The *E. coli* inner and outer membranes were isolated by a modified sucrose gradients centrifugation.[31] In brief, 3 mL of 60% (w/v) sucrose, 3 mL of 51% (w/v) sucrose, 3 mL of 36% (w/v) sucrose, and 4 mL of total membrane suspension (all in 20 mM Tris, pH 8.0, 100 mM NaCl) were poured in a stepwise manner from bottom to top of a centrifugation tube. The membrane suspension was mixed uniformly by a slight ultrasonication before centrifugation. After centrifugation at 210000*g* for 15 h by an SW-40 Ti rotor (Beckman), two clear membrane layers appeared at the sucrose interface. The golden yellow layer between 35% and 51% sucrose was inner membranes, and the white layer between 51% and 60% was outer membranes. The inner membranes were collected by centrifugation at 548352*g* for 3 h and washed three times with a buffer (10 mM Tris, pH 8.0, 25 mM NaCl). Finally, inner membranes containing ∼24 mg U-^{13}C,^{15}N-Δ4-AqpZ and 30% (w/w) hydration were packed into a thin-wall rotor for ssNMR experiments.

Water Permeability Measurements. Water permeability of wt- and Δ4-AqpZ POPC/POPG proteoliposomes was characterized as described in the literature.[29] In detail, the POPC/POPG blank liposomes and AqpZ and Δ4-AqpZ proteoliposomes (lipid/protein ratio of 10, w/w) were prepared by dialysis following the same procedure used to prepare the samples for NMR experiments. The water permeability of liposomes and proteoliposomes was measured by an SX20 stopped-flow spectrometer (Applied Photophysics, Leatherhead, UK) at a light source of 577 nm wavelength. After rapid mixture with hyperosmolar buffer (600 mM sucrose), the kinetics of increase in light scattering was recorded as a function of time. The average radius values of blank liposomes and AqpZ proteoliposomes were measured by dynamic light scattering. The water permeability (P_f) was fitted as described in the literature.[8]

ssNMR Experiments. The 2D/3D experiments for resonance assignments of U-^{13}C,^{15}N-AqpZ proteoliposomes were performed on a wide-bore Varian VNMRS NMR spectrometer operating at 600 MHz using a 4 mm triple-resonance T3-HXY MAS probe under 8 kHz spinning rate. In these ssNMR experiments, the selective polarization transfer between ^{13}C and ^{15}N was achieved by SPECIFIC CP,[32] and ^{13}C−^{13}C correlations were established through by dipolar assisted rotational resonance (DARR) recoupling.[33] The water−protein chemical exchange, Z-filtered transferred echo double resonance (ZF-TEDOR)[34]/NCO, and ^{1}H−^{15}N DIPSHIFT experiments[35] of U-^{13}C,^{15}N-Δ4-AqpZ in POPC/POPG proteoliposomes and *E. coli* membranes were carried out on a standard-bore Bruker Advance 800 MHz spectrometer with a 3.2 mm E-free HCN MAS probe. The water−protein chemical exchange experiments were carried out with the pulse sequence used by Fu et al.[36] Lee−Goldberg (LG) spin-lock times of 0.05, 0.5, 1, 3, 6, 10, 20, and 30 ms was used under ∼65 kHz ^{1}H effective radio frequency (RF) field. We obtained the ^{1}H $T_{1\rho}$ of AqpZ in separate experiments and then fitted the equation derived by Fu et al.[36] to yield exchange rate constants between hydronium ions and the protons in the R189 NH bonds. ^{1}H−^{15}N dipolar couplings of U-^{13}C,^{15}N-Δ4-AqpZ were obtained by using the R18$^{7}_{1}$recoupling[37] in the DIPSHIFT experiments at 8.9 kHz MAS spinning rate.

Typical 90° pulse lengths of 4.3 μs (^{1}H), 4.9 μs (^{13}C), and 6.0 μs (^{15}N) were used in MAS NMR experiments. The ∼65 kHz ^{1}H RF field was used for decoupling during the acquisition and indirect evolution periods in the 2D/3D experiments. The ^{13}C chemical shifts were referenced to adamantane used as external referencing standards (40.48 ppm for the methylene carbon[38]), and ^{15}N chemical shifts were indirectly referenced to liquid NH_3 according to gyromagnetic ratios. The NMR data were processed by NMRpipe[39] and analyzed by Sparky.

Theoretical Calculations, Lineshape Simulations, and Structure Calculations. All theoretical calculations were performed by Gaussian 09. The combined theoretical model, namely ONIOM (B3LYP/6-31G:MNDO)[40] was applied to predict the four monomers' geometries of fragments. In calculations, the R189 side chain and close atoms were set as the high-level layer, with the rest of the atoms in the low-level layer. All atoms except hydrogen atoms were ascertained by X-ray structure, and only hydrogen atoms were relaxed in both high and low layers. All magnetic shielding results were calculated on the basis of the gauge including atomic orbitals (GIAO)[41] formulation at the ONIOM(B3LYP/6-31G(d):B3LYP/3-21G) level of theory. The calculated ^{15}N chemical shifts were referenced to glycine.

The order parameter S is the ratio between the averaged anisotropy parameter $\bar{\delta}$ and the rigid-limit δ. The motionally averaged anisotropy parameter $\bar{\delta}$ was calculated as $\bar{\delta} \equiv |\bar{\omega}_n|_{max}$. The principal values of the motionally averaged tensor $\bar{\omega}_n$ are related to the torsion angle $\Delta\chi$ around a motional axis C_γ-C_δ.[42] The torsion angle $\Delta\chi$ was calculated by the flip angle β and the angle θ using the equation derived by Hong et al.[43] The flip angle β of 67° was obtained from molecular dynamics simulations of AqpZ,[10] and the angle θ, which is the angle between the motional axis C_γ−C_δ and the N_ε−H_ε bond, was obtained by translating the N_ε−H_ε bond from the N_ε atom to the C_δ atom along N_ε−C_δ bond of the X-ray structure (PDB entry 2ABM).[9] By this way, we can calculate the order parameters of the ^{1}H−^{15}N$_\varepsilon$ bond of 0.44, 0.54, 0.48, 0.52 for monomers A, B, C and D, respectively.

Numerical simulations of ^{1}H−^{15}N dipolar lineshapes were performed using SIMPSON software.[44] To extract the dipolar coupling constants, the same parameters as those in the ssNMR experiments (i.e., ^{1}H Larmor frequency, MAS frequency, RF field strength, number of t1 points, zero-filling, line broadening, etc.) were used in the simulations. Powder averaging was performed by using 400 bcr angles (α, β) and 16 γ angles. Isolated ^{1}H−^{15}N spin pairs were used in the simulations, and the effect of ^{1}H chemical shift anisotropy was taken into account (^{1}H CSA = 7.8 ppm, η = 0 for the proton atom connected to backbone ^{15}N, ^{1}H CSA = 11 ppm, η = 0 for the proton connected to Arg189 N_ε, the principal element δ_{zz} was along the ^{15}N−^{1}H bond). The dipolar coupling constants were extracted from the simulated dipolar lineshapes with the lowest sum of the squared errors.

The AqpZ monomeric structure calculations were performed using the standard POMONA/CS-RosettaCM protocol of the CS-Rosetta package.[45,46] As the inputs, only backbone ^{15}N, $^{13}C_\alpha$, ^{13}C′, and $^{13}C_\beta$ chemical shifts were used for the fragments and templates selection procedures. For the subsequent structure generation procedure, only those fragments and templates from PDB proteins with <30% sequence identity to the AqpZ protein were used, and those R189 side-chain-related experimental restraints were also included to generate in total 10 000 full-atom models, from which the 10 lowest energy models were selected as the calculated structures.

DOI: 10.1021/jacs.8b03446
J. Am. Chem. Soc. 2018, 140, 7885−7895

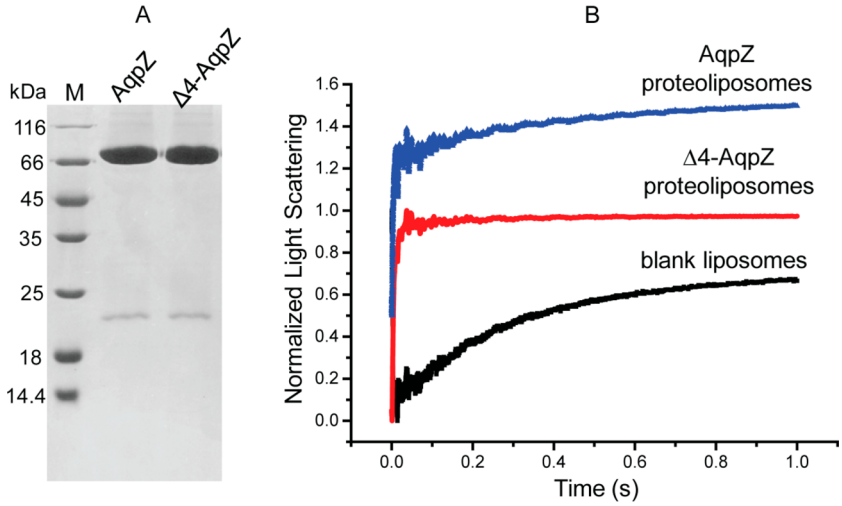

Figure 1. (A) SDS-PAGE of wild-type and Δ4-AqpZ in POPC/POPG proteoliposomes. (B) Light scattering traces of wild-type AqpZ (blue), Δ4-AqpZ reconstituted in POPC/POPG proteoliposomes (red), and protein-free liposomes suspensions (black) upon hypertonic shock produced in the stopped-flow apparatus. The much faster shrinking of AqpZ proteoliposomes than that of protein-free liposomes indicates high water permeability of AqpZ proteoliposomes.

RESULTS AND DISCUSSION

AqpZ Reconstituted in Synthetic Bilayers Is Functionally Active. We characterized the folding, oligomeric state and water permeability of AqpZ in POPC/POPG proteoliposomes to examine the reconstitution of AqpZ into synthetic bilayers. Circular dichroism (CD) spectra demonstrated that the reconstituted AqpZ is correctly folded as an α-helical structure (Figure S2). SDS-PAGE showed that AqpZ is a tetramer in lipid bilayers (Figure 1A), as that in the native environments. Water permeability of AqpZ proteoliposomes was measured using a stopped-flow apparatus.[8] As shown by the light scattering traces in Figure 1B, much faster shrinking of AqpZ proteoliposomes as compared to protein-free liposomes indicated high water permeability. Indeed, the osmotic water permeability (P_f) of AqpZ proteoliposomes was fitted to be 702 (10^{-4} cm/s), whereas P_f of the protein-free liposomes is 7.2 (10^{-4} cm/s), both are similar to those in the previous study.[8] The high water permeability, together with an analysis of CD and SDS-PAGE, suggested that AqpZ is correctly folded and functionally active in the synthetic bilayers.

TEDOR and NCO Spectra Reveal One Conformation of the R189 Side Chain in Synthetic Bilayers and Native Membranes. Chemical shift is very sensitive to the local chemical environments, thus can serve as a probe for local conformation of proteins. To identify the conformational state of the R189 side chain of AqpZ in the synthetic bilayers, we assigned chemical shifts of R189. Excellent resolution and sensitivity of ssNMR spectra of U-^{13}C,^{15}N-AqpZ proteoliposome sample allowed us to assign 218 out of 231 residues by a set of NCACX, NCOCX, and CONCA 3D experiments (BRMB #27244),[47] similar to that of Aqp1.[48] However, signals corresponding to the R189 side chain cannot be assigned by these 3D spectra. There are five arginine residues in AqpZ, whose NMR signals are too crowded in the N(CA)CX 2D spectrum and too weak in the NCACX (or NCOCX) 3D spectrum to be assigned. To obtain resonance assignments of the R189 side chain, all arginine residues except R189 were mutated to lysine residues. This mutant is referred to as Δ4-AqpZ in this study. Fortunately, as shown in Figure 1, the Δ4-AqpZ remains the similar oligomeric state and high water permeability as the wt-AqpZ. 2D ^{13}C−^{15}N TEDOR spectrum of U-^{13}C,^{15}N-Δ4-AqpZ was recorded. As shown in Figure 2A, the three isolated cross peaks along the characteristic chemical shift of $^{13}C_\zeta$ (δ = 159.1 ppm) of R189 in the spectrum were assigned to N_ε (δ = 87.4 ppm), $N_{\eta 1}$ (δ = 68.0 ppm) and $N_{\eta 2}$ (δ = 70.0 ppm) of R189, respectively. We examined the line widths and intensities of these three peaks and did not observe double or multiple-components. Peaks corresponding to N_ε, $N_{\eta 1}$, and $N_{\eta 2}$ are also well-resolved in 1D ^{15}N CP spectrum of U-^{13}C,^{15}N-Δ4-AqpZ. Thus, ^{15}N CP can be used to monitor a low population of the other stable conformation of the R189 side chain. As shown in Figure S3, the good signal-to-noise ratio (~100) of these narrow, symmetrical peaks indicates that there is no other stable conformation of the R189 side chain with >1% population.

To further characterize the conformation of the R189 side chain in native *E. coli* membranes, chemical shifts of the R189 side chain of AqpZ in the native inner *E. coli* membranes were assigned. *E. coli* membranes provide more native membrane environments in terms of lipid compositions, bilayer asymmetry, chemical gradients, and macromolecular crowding than the synthetic bilayers. Though ssNMR studies of several membrane proteins in native cellular membranes have been reported,[18,31,49−58] adequate spectral quality of ssNMR spectra of cellular membranes is still a challenge due to the low signal sensitivity of the target protein and serious interference of signals from background proteins as well as lipids. In this study, the samples of labeled Δ4-AqpZ in *E. coli* membranes were prepared using a "dual-media" method to label AqpZ selectively while to suppress the labeling of background proteins. In addition, the outer membranes without containing inner membrane protein AqpZ were removed by sucrose density gradient centrifugation to increase the content of AqpZ in the *E. coli* membranes in which AqpZ accounts for ~45% of the expressed proteins and ~80% of isotope-labeled protein (data not shown). Consequently, 2D spectra can be recorded with sufficient spectral quality due to high sensitivities benefitted from the overexpression of AqpZ (~40 mg/L in the M9 media) in the *E. coli* cells and the removal of the outer membranes. The 2D NCO spectrum of U-^{13}C,^{15}N-Δ4-AqpZ in *E. coli*

DOI: 10.1021/jacs.8b03446
J. Am. Chem. Soc. 2018, 140, 7885−7895

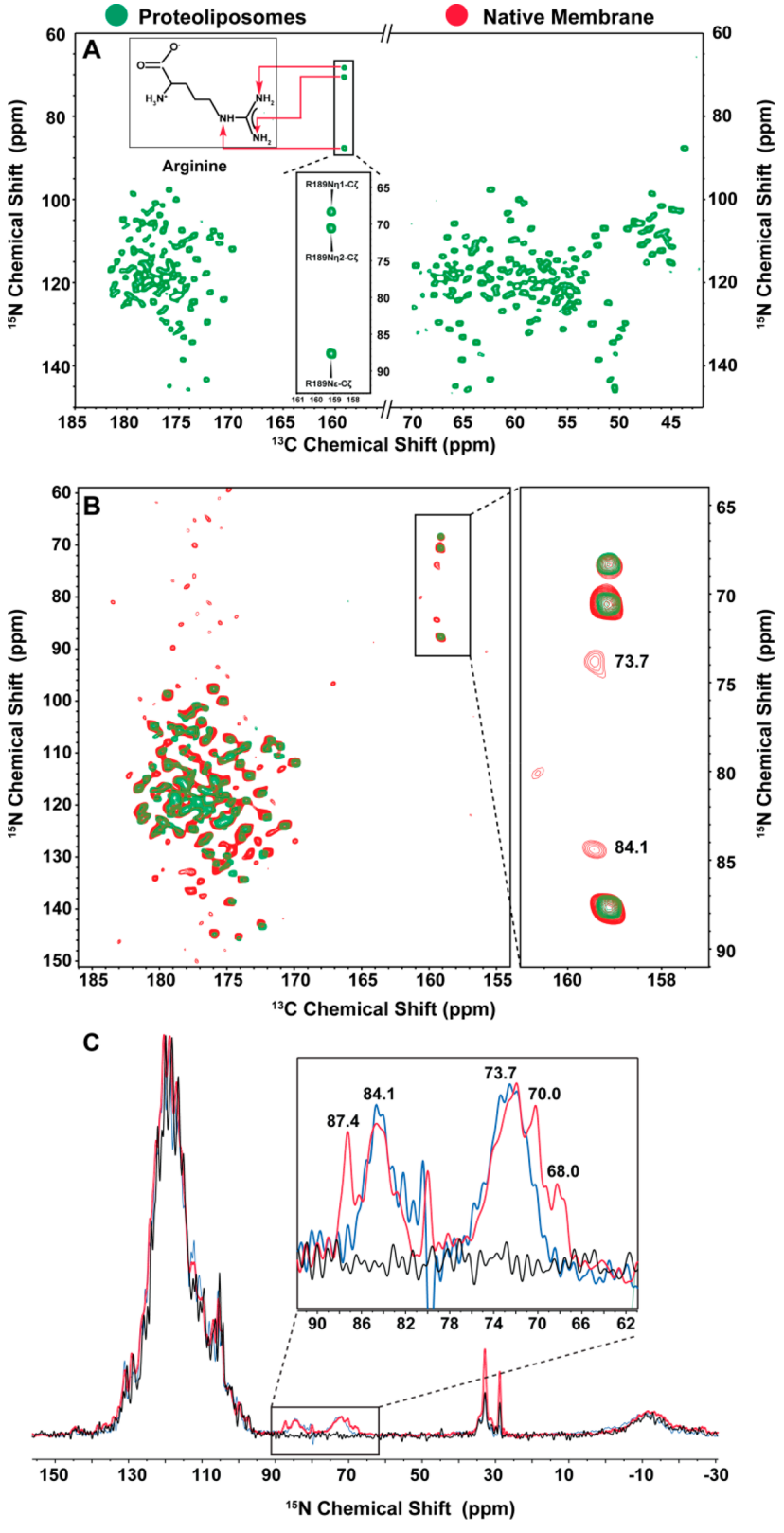

Figure 2. (A) 2D ^{15}N−^{13}C correlation TEDOR spectrum of U-^{13}C,^{15}N-Δ4-AqpZ in POPC/POPG proteoliposomes. (B) 2D NCO spectrum of U-^{13}C,^{15}N-Δ4-AqpZ in native membranes. For comparison, the corresponding region of TEDOR (green) of (A) is superimposed onto the NCO spectrum (red). (C) 1D ^{15}N CP spectra for assigning two peaks at ^{15}N δ = 73.7 and 84.1 ppm in (B) to arginine residues of background proteins. Spectra of Δ4-AqpZ, Δ5-AqpZ, and all arginine reverse-labeled (natural abundance) samples are shown in red, blue, and black, respectively.

membranes showed similarities to the corresponding region of the TEDOR spectrum in synthetic bilayers (Figure 2B), implying similar structures of AqpZ in the two environments. Three peaks corresponding to three ^{15}N atoms of the R189 side chain in NCO spectra are well superimposed with those in TEDOR spectrum. However, besides these three peaks, there

DOI: 10.1021/jacs.8b03446
J. Am. Chem. Soc. 2018, 140, 7885−7895

are two additional signals at ^{15}N δ = 73.7 and 84.1 ppm along with ^{13}C chemical shift slightly deviating 159.1 ppm of $^{13}C_\zeta$ of R189. To assign these two signals, we mutated all five arginine residues (including R189) of AqpZ (Δ5-AqpZ), and did not observe the disappearance of these two signals (Figure 2C, blue), suggesting these signals are not derived from AqpZ. Further, we reversely labeled arginine residues of all proteins by adding natural abundance arginine in the growing media, and found that all ^{15}N labeling of arginine residues was completely abolished (Figure 2C, black), indicating the two additional signals were derived from background proteins in *E. coli* membranes.

To investigate whether the open and closed conformations can be distinguished by chemical shifts, the chemical shifts of guanidino groups of R189 in one open monomer and three closed monomers of the X-ray structure were theoretically calculated (Figure S4). As listed in Table 1, the ^{15}N chemical shifts differences of three ^{15}N atoms of the R189 side chain between the open and closed conformations are apparently distinguishable with the minimal difference of 2.5 ppm. The calculated chemical shifts of N_ε in monomer A and $N_{\eta 2}$ in monomer D looked surprisingly larger than their counterparts in the other monomers. However, detailed examinations of the charge distribution, hydrogen types and lengths of these two ^{15}N atoms in the X-ray structure indicated that the calculated results are reliable, as shown in Figure S5. Therefore, if there were open and closed conformations of the R189 side chain, they should give rise to two sets of distinct peaks in TEDOR and NCO spectra, whereas only one set of peaks of the R189 side chain observed in ssNMR spectra suggested the presence of one stable conformation of the R189 side chain in the synthetic bilayers and native membranes.

Table 1. Theoretically Calculated ^{15}N Chemical Shifts of Atoms of the R189 Side Chain in Different Monomers in X-ray Structure (PDB Entry 2ABM)[9]

		^{15}N chemical shift (ppm)[a]		
monomer	conformation	N_ε	$N_{\eta 2}$	$N_{\eta 1}$
A	open	81.9	61.5	58.5
B	closed	73.5	77.2	66.3
C	closed	71.7	64.3	80.6
D	closed	66.4	64.0	123.2

[a]The uncertainty of calculated ^{15}N chemical shifts is ±1.9 ppm, which was estimated by a standard from the calculations of the chemical shifts in monomer A using the 6-311G(df,pd) basis set.

DIPSHIFT Spectra Suggest Immobility of the R189 Side Chain in Synthetic Bilayers and Native Membranes. To examine mobility of the R189 side chain, we measured the dipolar lineshape of $^1H-^{15}N_\varepsilon$ of R189 by 2D $^1H-^{15}N$ DIPSHIFT experiments. Dipolar couplings can be averaged by the large-amplitude motions with a rate faster than dipolar coupling interactions, thus motional-averaged dipolar lineshapes can be used to probe motions in the fast time scales. Thanks to the mutations of 4 arginine residues in Δ4-AqpZ, we can obtain isolated ^{15}N peaks of the R189 side chain in 1D $^1H-^{15}N$ CP spectrum, which allows us to record site-specific dipolar lineshapes of $^1H-^{15}N_\varepsilon$ by 2D $^1H-^{15}N$ DIPSHIFT spectra, while lineshape of $^1H-^{15}N_\eta$ cannot be obtained due to its low sensitivity. Dipolar coupling constants of 11.2 ± 0.3 and 10.9 ± 0.4 kHz were obtained by fitting from main-chain $^1H-^{15}N$ (^{15}N δ = 120.0 ppm) and R189 side-chain $^1H-^{15}N_\varepsilon$ lineshapes (Figures 3 and S6), respectively. Both are close to the rigid limit of 11.3 kHz,[59] suggesting the immobility of the main chain and the R189 side chain.

Dynamics of the R189 side chain can be affected by the compositions and phase/temperature of the lipids. To

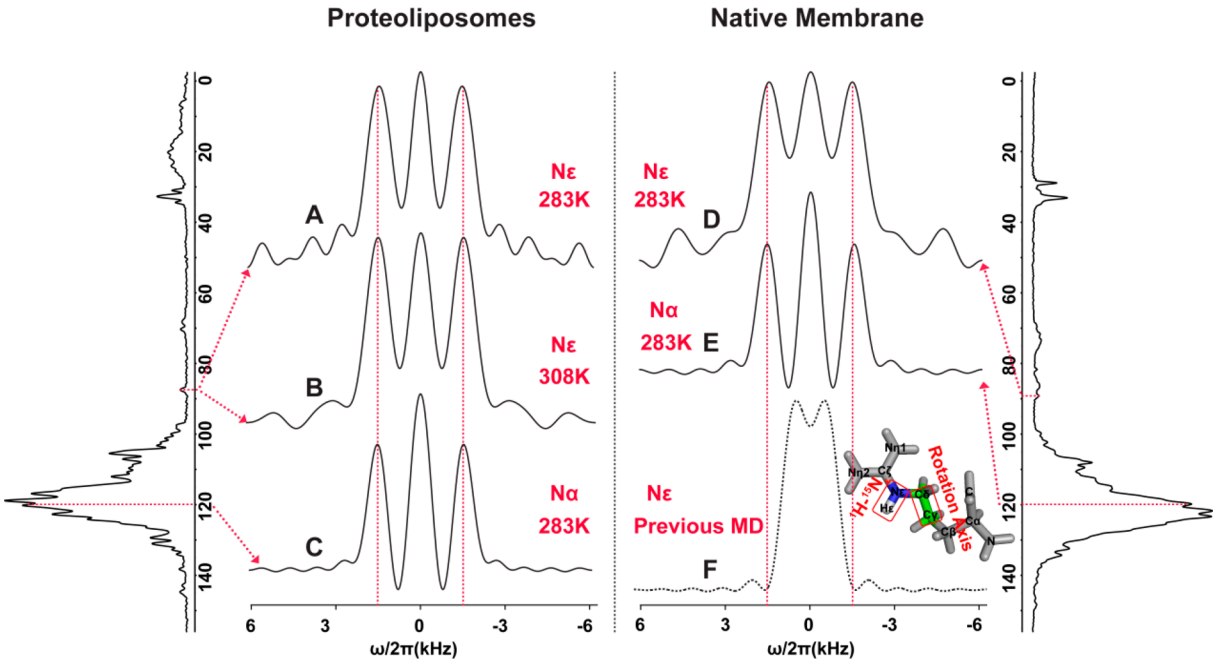

Figure 3. 2D $^1H-^{15}N$ DIPSHIFT spectra of U-^{13}C,^{15}N-Δ4-AqpZ in POPC/POPG proteoliposomes (A–C) and in native membranes (D,E). $^1H-^{15}N$ dipolar lineshapes of main-chain ^{15}N and R189 side-chain $^{15}N_\varepsilon$ were extracted from the spectra. The $^1H-^{15}N_\varepsilon$ dipolar lineshape (F, dashed line) was simulated on the basis of the model of the conformational switches between the open and closed states of the R189 side chain as suggested by the previous MD study.[10] The axis of $^1H-^{15}N_\varepsilon$ rotation along $C_\gamma-C_\delta$ is also shown in (F).

DOI: 10.1021/jacs.8b03446
J. Am. Chem. Soc. 2018, 140, 7885–7895

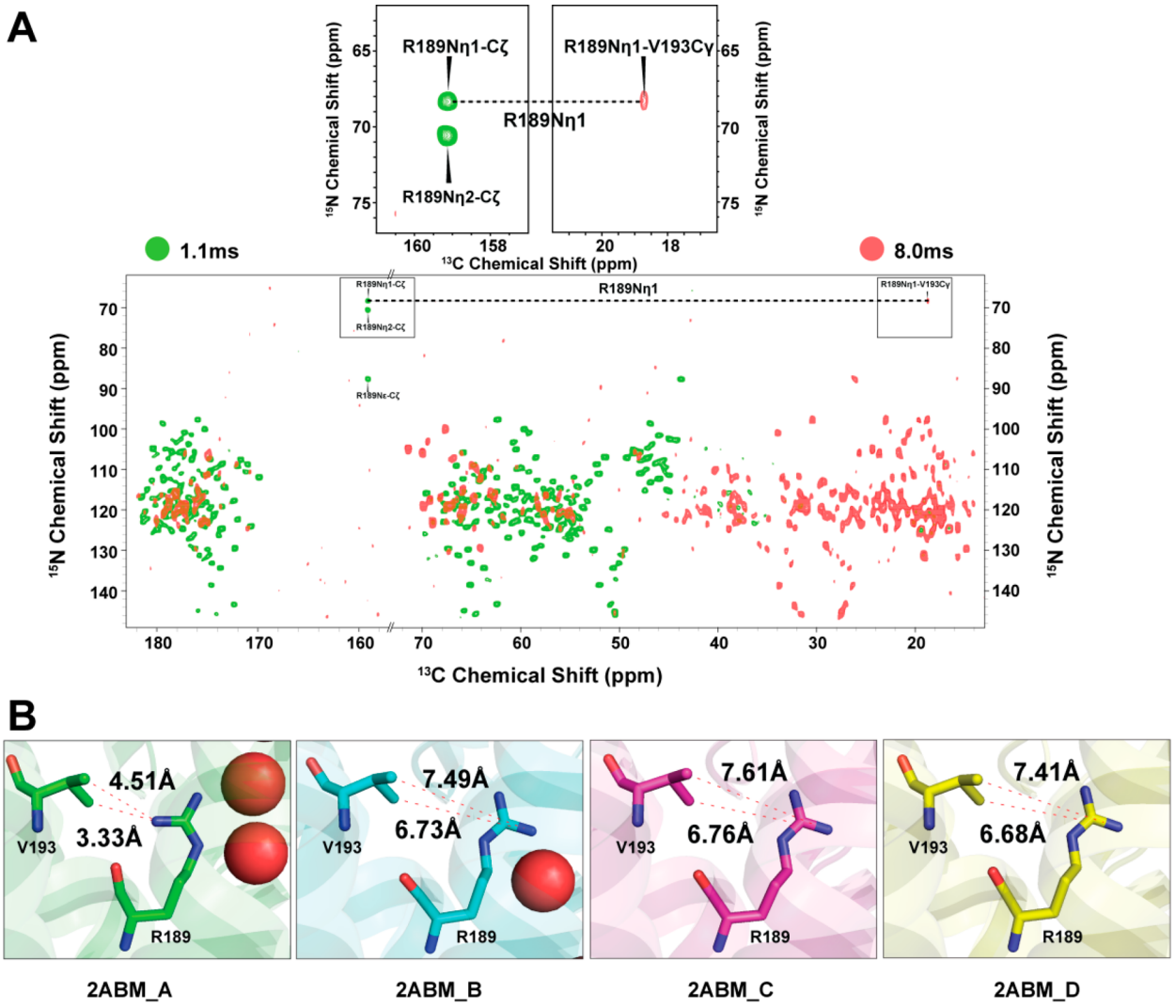

Figure 4. (A) 2D ^{15}N−^{13}C ZF-TEDOR spectrum with 8.0 ms (red) mixing time of U-^{13}C,^{15}N-Δ4-AqpZ for assigning distance restraints related to the R189 side chain. For comparison, the spectrum with 1.1 ms (green) mixing time is superimposed onto that with 8.0 ms. The cross peak (^{15}N δ = 87.4 ppm, ^{13}C δ = 17.4 ppm) in the spectrum with 8.0 ms mixing time can be assigned unambiguously to a correlation between N_ε of R189 and $C_{\gamma1}$/$C_{\gamma2}$ of V193. (B) Distances between N_ε of R189 and C_γ of V193 in the four monomers (2ABM_A, B, C, and D) of the X-ray structure.[9]

investigate the influence of compositions and phase of lipids to the mobility of the R189 side chain, we examined the mobility of the R189 side chain at different conditions. In the *E. coli* inner membranes which represent a native membrane environment of AqpZ, the dipolar lineshape of R189 ^{1}H−$^{15}N_\varepsilon$ was fitted with a dipolar coupling constant of 10.8 ± 0.5 kHz, indicative of the similar immobility as that in the synthetic bilayers. In the liquid-crystal phase of the POPC/POPG lipids as demonstrated by the ^{1}H line widths of CH_2 groups at 308 K (Figure S6), the dipolar splitting of R189 ^{1}H−$^{15}N_\varepsilon$ was observed almost the same as that in the gel phase at 298 K, as shown in Figure 3, suggesting immobility of the R189 side chain in both the gel and liquid-crystal phases of lipids.

Previous MD study observed rapid flips between the open and closed conformations of the R189 side chain on the nanosecond time scale, with a variation of its dihedral angle C_β−C_γ−C_δ−N_ε from −165.4° in the open conformation to −98.4° in the closed conformation.[10] If the large-amplitude conformational flips occurred, they should average ^{1}H−$^{15}N_\varepsilon$ dipolar coupling significantly. Thus motional-averaged ^{1}H−$^{15}N_\varepsilon$ lineshape was simulated on the basis of the orientation and amplitude of the motions suggested by the previous MD study[10] (Figure S8), as shown by the dashed line in Figure 3F. Indeed, flips of the R189 side chain lead to a significant narrowing of the ^{1}H−$^{15}N_\varepsilon$ lineshape compared to experimentally observed lineshapes. Therefore, a series of 2D DIPSHIFT experiments suggested no existence of the rapid conformational switches of the R189 side chain in the synthetic bilayers and native membranes.

Distance Restraints Related to the R189 Side Chain from TEDOR and PDSD Spectra. With nearly complete resonance assignments, 3D structural models of AqpZ can be constructed by powerful CS-Rosetta method.[45,46] Though a tetrameric structure cannot be built due to high complexity of the sampling, the high-resolution monomeric full-atom structure of AqpZ can be obtained by CS-Rosetta using nearly complete backbone and $^{13}C_\beta$ chemical shift assignments. Due to the presence of the water pore and the lack of structural restraints, the conformation of the side chain in the molecular core, in particular that of the R189 side chain, is less restrained during the last step of side-chain packing and full-atom refinement of CS-Rosetta structure generation. To refine the

DOI: 10.1021/jacs.8b03446
J. Am. Chem. Soc. 2018, 140, 7885−7895

conformation of the R189 side chain in the structure calculations, we measured a number of distance restraints related to the R189 side chain using 2D $^{15}N-^{13}C$ TEDOR and $^{13}C-^{13}C$ proton driven spin diffusion (PDSD) spectra of U-^{13}C,^{15}N-Δ4-AqpZ proteoliposomes. In the 2D TEDOR spectrum with 8.0 ms mixing time as shown in Figure 4A, the cross peak (^{15}N δ = 87.4 ppm, ^{13}C δ = 17.4 ppm) can be assigned unambiguously to a correlation between N_ε of R189 and $C_{\gamma1}/C_{\gamma2}$ of V193. This cross peak was observed repeatedly in the 2D TEDOR spectrum with 6.8 ms mixing time as shown in Figure S9 of the Supporting Information. The presence of this peak in both TEDOR spectra with 6.8 and 8.0 ms mixing time suggested a distance of R189N_ε–V193$C_{\gamma1}/C_{\gamma2}$ with less than 6.0 Å.[60] As shown in Figure 4B, this restraint is consistent with the 3.33/4.51 Å distance of R189N_ε–V193$C_{\gamma1}/C_{\gamma2}$ in the open monomer A of the X-ray structure, whereas is not consistent with those of 6.73/7.49, 6.76/7.61, and 6.68/7.41 Å in the closed monomers B, C, and D, respectively. In addition, the unique chemical shift of R189 C_ζ (^{13}C δ = 159.1 ppm) allows us to assign 14 unambiguous and 15 ambiguous $^{13}C_\zeta-^{13}C$ distance restraints in the 2D $^{13}C-^{13}C$ PDSD spectra with a mixing time of 250, 350, 500, and 1000 ms, respectively, as shown in Figures 5 and S10. All the distance restraints related to the R189 side chain are listed in Table S2.

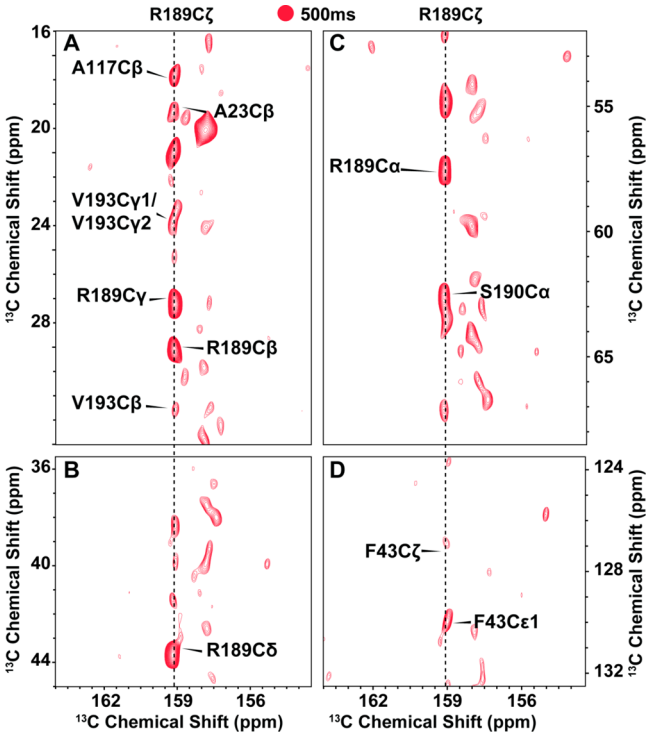

Figure 5. Representative region of 2D $^{13}C-^{13}C$ PDSD spectra with mixing time of 500 ms. The unique chemical shift of R189 C_ζ (^{13}C δ = 159.1 ppm) allowed us to assign a number of $^{13}C_\zeta-^{13}C$ distance restraints. Only unambiguously assigned distance restraints are labeled in this figure.

3D ssNMR Structure of AqpZ Indicates That the R189 Side Chain Is in an Open Conformation. Using nearly complete backbone and $^{13}C_\beta$ chemical shift assignments and 30 experimentally measured distance restraints related to the R189 side chain, high-resolution 3D monomeric structures of AqpZ were determined by CS-Rosetta to reveal conformation of the R189 side chain within the water channel. The 10 structural models with the lowest energy among 10 000 CS-Rosetta calculated structures are shown in Figure 6. These 10 structures are highly converged with an averaged C_α RMSD of 0.80 Å relative to the mean structure (Figure 6A). An averaged C_α RMSD of 1.27 Å relative to the X-ray structure (PDB entry 1RC2) indicates similarity of ssNMR and X-ray structures (Figure 6C). In the X-ray structure, the guanidino group of R189 adopts an orientation up toward the extracellular side in the open conformation, while it adopts an orientation down toward the channel in the closed conformation.[9] In these 10 ssNMR structures, the R189 side chain turns away from the channel pore, adopting a conformation similar to the upward/open conformation of the X-ray structure though the orientation of guanidino group of these structures showed some degree of dispersion in the direction perpendicular to water channel (Figure 6B). Apparently, water channels are open in the SF constriction region in all the 10 structures with the narrowest size of 3.29 Å, sufficient for passing through water molecules. The open structure is consistent with the other ssNMR experimental results and the water permeability essay. Since there is only one stable conformation of the R189 side chain as demonstrated by TEDOR and NCO experiments and the channel is highly permeable for water, the channels should be open in all monomers of AqpZ. All 10 structures have 2–4 hydrogen bonds between $N_\eta H_2$ of R189 and main-chain carboxyl oxygen of A117, T183, S184 and N119, stabilizing guanidino group of R189 to an orientation roughly parallel to the water channel (Table S3). The typical ssNMR structure (S0306 in Table S3) among the 10 structures is shown in Figure 7.

Water–Chemical Exchange Experiments Verify the Open Conformation of the R189 Side Chain. Water accessibility of the R189 side chain is different in the open and closed monomers in the X-ray structure. The R189 side chain can be accessed by water molecules in the open structure, while the SF is blocked and the R189 side chain cannot be accessed in the closed structure.[9] Therefore water accessibility can be used to verify the conformation of the R189 side chain. The water accessibility of the R189 side chain was probed by measuring water–protein chemical exchange rate constants using the method recently proposed by Fu et al.[36] Three peaks corresponding to three ^{15}N atoms of the R189 side chain are well resolved in 1D ^{15}N CP spectrum, enabling us to measure site-specific water–protein chemical exchange rate constants of protons connected to these ^{15}N atoms. As shown in Figure 8, the protons of N_ε and $N_{\eta2}$ sites are in exchange with water at rate constants of 155 ± 30 and 33 ± 19 s^{-1}, respectively, whereas the $N_{\eta1}$ site shows much slower exchange between its proton and water at a rate constant of 0.006 ± 0.04 s^{-1}, implying that this site is almost inaccessible by water. These water accessibilities revealed by the water–protein exchange rate constants are consistent with the open conformation of the R189 side chain in the ssNMR structure. As shown in Figure 7, N_ε and $N_{\eta2}$ of R189 face the channel pore in the ssNMR structure, and should be accessible by water, whereas $N_{\eta1}$ of R189 is partially shielded by $N_{\eta2}$ from the water channel and may have steric hindrance accessed by water molecules. Though the quantitative interpretation of the exchange rate constant of $N_{\eta1}$ is difficult,[61] an average of ~1 Å farther away of $N_{\eta1}$ than $N_{\eta2}$ from the water channel in the 10 ssNMR structures should be one of the factors contributing to the difference in their water accessibilities. The detailed distances of

DOI: 10.1021/jacs.8b03446
J. Am. Chem. Soc. 2018, 140, 7885–7895

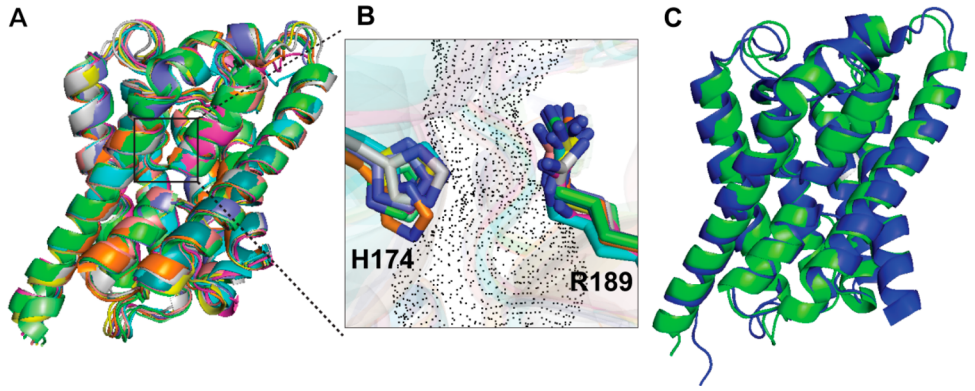

Figure 6. (A) Superimposing of 10 ssNMR structures of AqpZ with the lowest energy demonstrating high converge of these structures. (B) guanidino groups of R189 in all ssNMR structures of AqpZ adopt an open conformation with the orientation roughly parallel to the water channel. (C) overlapping of a ssNMR structure into X-ray structure[62] showing the similarity of the two structures. The water channel in (B) was predicted by Hollow software[65] using a ssNMR structure.

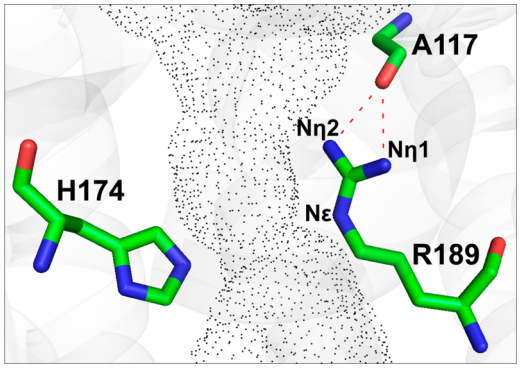

Figure 7. Selective filter region of a typical ssNMR structure (S3060). There are two hydrogen bonds stabilizing the R189 side chain into an orientation roughly parallel to the water channel. N_{ε} and $N_{\eta 2}$ of the R189 side chain face the channel pore, while $N_{\eta 1}$ is partially on the back of the water pore. The water channel was predicted by HOLE software[65] using a ssNMR structure.

$N_{\eta 1}$ away from the water channel compared to $N_{\eta 2}$ in the 10 ssNMR structures are listed in Table S3.

Gating Mechanism of the R189 Side Chain of AqpZ in Synthetic Bilayers and Native Membranes Examined by ssNMR. Two features are defined for a gate: (1) the presence of open and closed states and (2) the switching between the open and closed states. Our ssNMR experimental results revealed that the R189 side chain of AqpZ does not possess these two features in the native and native-like membrane environments.

One of the key observations of this study is the presence of a single conformation of the R189 side chain of AqpZ in the synthetic bilayers and native *E. coli* membranes. Though R189 is in the middle of AqpZ, its conformation can be affected by residues on the surface and the membrane (detergent) environment. Dual conformations of the R189 side chain observed in the X-ray structure is likely due to a perturbation of non-native detergent environments or asymmetric crystal packing contact.[9] It should be noted that structural perturbation by non-native environments was present not only in the X-ray structure of AqpZ (PDB entry 2ABM), but also in other X-ray structure of AqpZ (PDB entry 1RC2). In the structure of AqpZ (PDB entry 1RC2),[62] there were apparent structural differences between homotetramer protomers A and B, likely due to crystal packing contact. If these

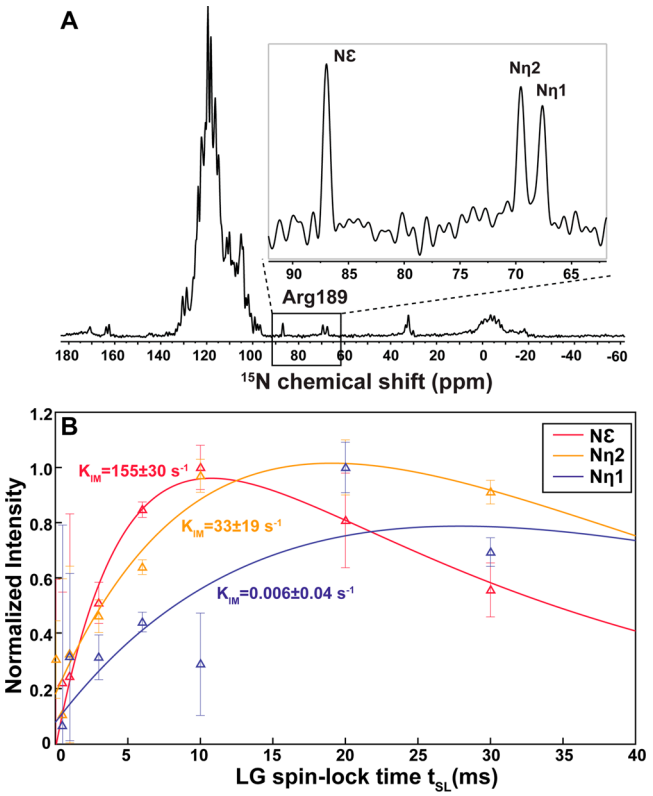

Figure 8. (A)[15] CP spectra of U-^{13}C,^{15}N-Δ4-AqpZ in POPC/POPG proteoliposomes, in which signals of N_{ε}, $N_{\eta 1}$, and $N_{\eta 2}$ of R189 can be resolved. (B) Normalized intensities of ^{15}N atoms of the R189 side chain as a function of Lee−Goldberg (LG) spin-lock times for fitting water−protein chemical exchange rate constants.

structural differences derived from non-native environmental factors were interpreted as different functional states of the protein, it may lead to misinterpretation of the structural mechanism. In contrast, in functionally active synthetic bilayers and native *E. coli* membranes, the observation of a single conformation of the R189 side chain in TEDOR and NCO spectra is free of perturbation of non-native mimetic environment and thus is valid.

Another important observation of this study is the immobility of the R189 side chain of AqpZ in the synthetic bilayers and *E. coli* membranes. Though MD studies

DOI: 10.1021/jacs.8b03446
J. Am. Chem. Soc. 2018, 140, 7885−7895

demonstrated the excessively high dynamics of the R189 side chain in AqpZ[11] or equivalent arginine residues in the other AQPs,[63] so far there has not been any experimental data supporting such a high flexibility of the R189 side chain. In contrast, B-factors of the R189 side chain and equivalent arginine residues in the X-ray structures of all AQPs showed no unusual high dynamics of the R189 side chain and equivalent residues. As shown in Table S1, the B-factors of the R189 side chain and equivalent arginine residues are similar to (or lower than) the average values of the side chain of other residues of AQPs. Consistent with X-ray B-factors, our DIPSHIFT experiments further revealed the immobility of the R189 side chain in native or native-like membranes at physiological temperature and the liquid-crystal phase of lipids. The immobility of the R189 side chain is inherently attributed to stabilization of the hydrogen bonds between $N_\eta H_2$ of R189 and carboxyl oxygen of A117 or other residues. These hydrogen bonds stabilizing the R189 side-chain orientation are present in all X-ray structures of AQPs including two X-ray structures of AqpZ, as also listed in Table S2, resulting in its low mobility in all X-ray structures as shown by their B-factors.

Most AQPs function as the permanently open channels for water permeation without a gate within the water channel.[64] Conformation, mobility, structure and water accessibility of the R189 side chain revealed by our ssNMR experiments, combining with water permeation essay, implied a permanently open conformation of the R189 side chain of AqpZ in native or native-like membrane environments. This study highlighted the importance of lipid bilayer environments in the molecular mechanism studies of membrane proteins. We note that caution should be taken to avoid misinterpretation of structural mechanism of membrane proteins in non-native mimetic environments. Finally, this study also demonstrated the power of ssNMR techniques in elucidating the molecular mechanism of membrane proteins in native or native-like membrane environments.

CONCLUSIONS

The gating mechanism of the R189 side chain of AqpZ in the synthetic bilayers and native *E. coli* membranes has been examined by ssNMR spectroscopy. 2D TEDOR and NCO spectra showed one set of peaks corresponding to the R189 side chain in lipid bilayers and *E. coli* membranes, respectively, suggesting a single stable conformation of R189 side chains. DIPSHIFT spectra suggested the immobility of the R189 side chain, thus excluding the possibility of the rapid switching of the R189 side chain between two conformations. High-resolution monomeric structure of AqpZ has been determined by CS-Rosetta calculations using a number of experimentally measured distance restraints related to the R189 side chain. In the ssNMR structures hydrogen bonds between NH_2 of R189 and carboxyl oxygen of A117 and other residues stabilize the R189 side chain in an open conformation with the orientation of its guanidino group roughly parallel to the pore of AqpZ. The open conformation of the R189 side chain has been verified by the presence of chemical exchange of water with protons of N_ε and $N_{\eta 2}$ of the R189 side chain facing the water pore, and very slow exchange of water with protons of $N_{\eta 1}$ back to the pore. All the solid-state NMR experimental results supported a permanently open conformation of the R189 side chain. The study has provided new insights into the gating mechanism of AQPs and highlighted the significance of lipid bilayer environments in the molecular mechanism studies of membrane proteins.

ASSOCIATED CONTENT

Supporting Information

The Supporting Information is available free of charge on the ACS Publications website at DOI: 10.1021/jacs.8b03446.

EM of proteoliposomes, CD spectrum of AqpZ, ^{15}N CP spectrum of Δ4-AqpZ, models for chemical shift calculations, calculated models of the R189 side chain, experimental and fitted $^1H-^{15}N$ dipolar lineshapes, line widths of ^1H MAS NMR peaks of lipids CH_2, models for calculations of order parameters, TEDOR and PDSD spectra with different mixing times, B-factors and hydrogen bonds of R189 in aquaporins, distance restraints related to the R189 side chain, and analysis of the water channel diameter in 10 ssNMR structures, including Figures S1−S10 and Tables S1−S3 (PDF)

AUTHOR INFORMATION

Corresponding Authors

*jufwang@scut.edu.cn
*yangjun@wipm.ac.cn

ORCID

Zhengfeng Zhang: 0000-0003-2025-8327
Anmin Zheng: 0000-0001-7115-6510
Riqiang Fu: 0000-0003-0075-0410
Jun Yang: 0000-0002-4480-5340

Author Contributions

⊗Y.Z. and H.X. contributed equally.

Notes

The authors declare no competing financial interest.

ACKNOWLEDGMENTS

This work is supported by grants from the National Natural Science Foundation of China (21425523, 31770798, 21405171, 21775161) and from the National Key R&D Program of China (2016YFA0501200, 2017YFA0505400). R.F. also wishes to acknowledge support from the National High Magnetic Field Laboratory (NHMFL), which is supported by the NSF Cooperative Agreement No. DMR-1644779 and the State of Florida.

REFERENCES

(1) Zhou, H. X.; Cross, T. A. *Annu. Rev. Biophys.* **2013**, *42*, 361−392.
(2) Cross, T. A.; Murray, D. T.; Watts, A. *Eur. Biophys. J.* **2013**, *42*, 731−755.
(3) Agre, P.; King, L. S.; Yasui, M.; Guggino, W. B.; Ottersen, O. P.; Fujiyoshi, Y.; Engel, A.; Nielsen, S. *J. Physiol.* **2002**, *542*, 3−16.
(4) Borgnia, M.; Nielsen, S.; Engel, A.; Agre, P. *Annu. Rev. Biochem.* **1999**, *68*, 425−458.
(5) Tornroth-Horsefield, S.; Hedfalk, K.; Fischer, G.; Lindkvist-Petersson, K.; Neutze, R. *FEBS Lett.* **2010**, *584*, 2580−2588.
(6) Hedfalk, K.; Tornroth-Horsefield, S.; Nyblom, M.; Johanson, U.; Kjellbom, P.; Neutze, R. *Curr. Opin. Struct. Biol.* **2006**, *16*, 447−456.
(7) Borgnia, M. J.; Agre, P. *Proc. Natl. Acad. Sci. U. S. A.* **2001**, *98*, 2888−2893.
(8) Borgnia, M. J.; Kozono, D.; Calamita, G.; Maloney, P. C.; Agre, P. *J. Mol. Biol.* **1999**, *291*, 1169−1179.
(9) Jiang, J. S.; Daniels, B. V.; Fu, D. *J. Biol. Chem.* **2006**, *281*, 454−460.
(10) Jensen, M. O.; Mouritsen, O. G. *Biophys. J.* **2006**, *90*, 2270−2284.

DOI: 10.1021/jacs.8b03446
J. Am. Chem. Soc. 2018, 140, 7885−7895

(11) Wang, Y.; Schulten, K.; Tajkhorshid, E. *Structure* **2005**, *13*, 1107−1118.
(12) Liang, R. B.; Swanson, J. M. J.; Madsen, J. J.; Hong, M.; DeGrado, W. F.; Voth, G. A. *Proc. Natl. Acad. Sci. U. S. A.* **2016**, *113*, E6955−E6964.
(13) Hong, M. *Biophys. J.* **2014**, *106*, 11a−11a.
(14) Baker, L. A.; Baldus, M. *Curr. Opin. Struct. Biol.* **2014**, *27*, 48−55.
(15) Williams, J. K.; Zhang, Y.; Schmidt-Rohr, K.; Hong, M. *Biophys. J.* **2013**, *104*, 1698−1708.
(16) Weingarth, M.; Prokofyev, A.; van der Cruijsen, E. A. W.; Nand, D.; Bonvin, A. M. J. J.; Pongs, O.; Baldus, M. *J. Am. Chem. Soc.* **2013**, *135*, 3983−3988.
(17) Gustavsson, M.; Verardi, R.; Mullen, D. G.; Mote, K. R.; Traaseth, N. J.; Gopinath, T.; Veglia, G. *Proc. Natl. Acad. Sci. U. S. A.* **2013**, *110*, 17338−17343.
(18) Miao, Y. M.; Qin, H. J.; Fu, R. Q.; Sharma, M.; Can, T. V.; Hung, I.; Luca, S.; Gor'kov, P. L.; Brey, W. W.; Cross, T. A. *Angew. Chem., Int. Ed.* **2012**, *51*, 8383−8386.
(19) Hong, M.; Fritzsching, K. J.; Williams, J. K. *J. Am. Chem. Soc.* **2012**, *134*, 14753−14755.
(20) Can, T. V.; Sharma, M.; Hung, I.; Gor'kov, P. L.; Brey, W. W.; Cross, T. A. *J. Am. Chem. Soc.* **2012**, *134*, 9022−9025.
(21) Ullrich, S. J.; Hellmich, U. A.; Ullrich, S.; Glaubitz, C. *Nat. Chem. Biol.* **2011**, *7*, 263−270.
(22) Palmer, A. G.; Williams, J.; McDermott, A. *J. Phys. Chem.* **1996**, *100*, 13293−13310.
(23) Good, D. B.; Wang, S. L.; Ward, M. E.; Struppe, J.; Brown, L. S.; Lewandowski, J. R.; Ladizhansky, V. *J. Am. Chem. Soc.* **2014**, *136*, 2833−2842.
(24) Huster, D.; Xiao, L. S.; Hong, M. *Biochemistry* **2001**, *40*, 7662−7674.
(25) Retel, J. S.; Nieuwkoop, A. J.; Hiller, M.; Higman, V. A.; Barbet-Massin, E.; Stanek, J.; Andreas, L. B.; Franks, W. T.; van Rossum, B. J.; Vinothkumar, K. R.; Handel, L.; de Palma, G. G.; Bardiaux, B.; Pintacuda, G.; Emsley, L.; Kuhlbrandt, W.; Oschkinat, H. *Nat. Commun.* **2017**, *8*, 2073.
(26) Das, N.; Dai, J.; Hung, I.; Rajagopalan, M. R.; Zhou, H. X.; Cross, T. A. *Proc. Natl. Acad. Sci. U. S. A.* **2015**, *112*, E119−E126.
(27) Wang, S. L.; Munro, R. A.; Shi, L. C.; Kawamura, I.; Okitsu, T.; Wada, A.; Kim, S. Y.; Jung, K. H.; Brown, L. S.; Ladizhansky, V. *Nat. Methods* **2013**, *10*, 1007−1012.
(28) Lu, G. J.; Tian, Y.; Vora, N.; Marassi, F. M.; Opella, S. J. *J. Am. Chem. Soc.* **2013**, *135*, 9299−9302.
(29) Wang, L. L.; Zhou, H.; Li, Z. J.; Lim, T. K.; Lim, X. S.; Lin, Q. S. *Protein Expression Purif.* **2015**, *115*, 146−152.
(30) Marley, J.; Lu, M.; Bracken, C. *J. Biomol. NMR* **2001**, *20*, 71−75.
(31) Baker, L. A.; Daniels, M.; van der Cruijsen, E. A. W.; Folkers, G. E.; Baldus, M. *J. Biomol. NMR* **2015**, *62*, 199−208.
(32) Baldus, M.; Petkova, A. T.; Herzfeld, J.; Griffin, R. G. *Mol. Phys.* **1998**, *95*, 1197−1207.
(33) Takegoshi, K.; Nakamura, S.; Terao, T. *Chem. Phys. Lett.* **2001**, *344*, 631−637.
(34) Jaroniec, C. P.; Filip, C.; Griffin, R. G. *J. Am. Chem. Soc.* **2002**, *124*, 10728−10742.
(35) Aue, W. P.; Ruben, D. J.; Griffin, R. G. *J. Magn. Reson.* **1981**, *43*, 472−477.
(36) Fu, R. Q.; Miao, Y. M.; Qin, H. J.; Cross, T. A. *J. Am. Chem. Soc.* **2016**, *138*, 15801−15804.
(37) Zhao, X.; Eden, M.; Levitt, M. H. *Chem. Phys. Lett.* **2001**, *342*, 353−361.
(38) Morcombe, C. R.; Zilm, K. W. *J. Magn. Reson.* **2003**, *162*, 479−486.
(39) Delaglio, F.; Grzesiek, S.; Vuister, G. W.; Zhu, G.; Pfeifer, J.; Bax, A. *J. Biomol. NMR* **1995**, *6*, 277−293.
(40) Dapprich, S.; Komaromi, I.; Byun, K. S.; Morokuma, K.; Frisch, M. J. *J. Mol. Struct.: THEOCHEM* **1999**, *461*, 1−21.
(41) Schreckenbach, G.; Ziegler, T. *J. Phys. Chem.* **1995**, *99*, 606−611.
(42) Hu, F.; Luo, W.; Hong, M. *Science* **2010**, *330*, 505−508.
(43) Cady, S. D.; Schmidt-Rohr, K.; Wang, J.; Soto, C. S.; DeGrado, W. F.; Hong, M. *Nature* **2010**, *463*, 689−692.
(44) Bak, M.; Rasmussen, J. T.; Nielsen, N. C. *J. Magn. Reson.* **2000**, *147*, 296−330.
(45) Shen, Y.; Bax, A. *Nat. Methods* **2015**, *12*, 747−750.
(46) Shen, Y.; Lange, O.; Delaglio, F.; Rossi, P.; Aramini, J. M.; Liu, G. H.; Eletsky, A.; Wu, Y. B.; Singarapu, K. K.; Lemak, A.; Ignatchenko, A.; Arrowsmith, C. H.; Szyperski, T.; Montelione, G. T.; Baker, D.; Bax, A. *Proc. Natl. Acad. Sci. U. S. A.* **2008**, *105*, 4685−4690.
(47) Xie, H. Y.; Zhao, Y. X.; Wang, J.; Zhang, Z. F.; Yang, J., *submitted*.
(48) Wang, S. L.; Ing, C.; Emami, S.; Jiang, Y. J.; Liang, H. J.; Pomes, R.; Brown, L. S.; Ladizhansky, V. *J. Phys. Chem. B* **2016**, *120*, 9887−9902.
(49) Warnet, X. L.; Laadhari, M.; Arnold, A. A.; Marcotte, I.; Warschawski, D. E. *Biochim. Biophys. Acta, Biomembr.* **2016**, *1858*, 146−152.
(50) Kaplan, M.; Narasimhan, S.; de Heus, C.; Mance, D.; van Doorn, S.; Houben, K.; Popov-Celeketic, D.; Damman, R.; Katrukha, E. A.; Jain, P.; Geerts, W. J. C.; Heck, A. J. R.; Folkers, G. E.; Kapitein, L. C.; Lemeer, S.; van Bergen en Henegouwen, P. M. P.; Baldus, M. *Cell* **2016**, *167*, 1241−1251.
(51) Yamamoto, K.; Caporini, M. A.; Im, S. C.; Waskell, L.; Ramamoorthy, A. *Biochim. Biophys. Acta, Biomembr.* **2015**, *1848*, 342−349.
(52) Ward, M. E.; Wang, S. L.; Munro, R.; Ritz, E.; Hung, I.; Gor'kov, P. L.; Jiang, Y. J.; Liang, H. J.; Brown, L. S.; Ladizhansky, V. *Biophys. J.* **2015**, *108*, 1683−1696.
(53) Renault, M.; Tommassen-van Boxtel, R.; Bos, M. P.; Post, J. A.; Tommassen, J.; Baldus, M. *Proc. Natl. Acad. Sci. U. S. A.* **2012**, *109*, 4863−4868.
(54) Fu, R. Q.; Wang, X. S.; Li, C. G.; Santiago-Miranda, A. N.; Pielak, G. J.; Tian, F. *J. Am. Chem. Soc.* **2011**, *133*, 12370−12373.
(55) Baker, L. A.; Sinnige, T.; Schellenberger, P.; de Keyzer, J.; Siebert, C. A.; Driessen, A. J. M.; Baldus, M.; Grunewald, K. *Structure* **2018**, *26*, 161−170.
(56) Shahid, S. A.; Nagaraj, M.; Chauhan, N.; Franks, T. W.; Bardiaux, B.; Habeck, M.; Orwick-Rydmark, M.; Linke, D.; van Rossum, B. J. *Angew. Chem., Int. Ed.* **2015**, *54*, 12602−12606.
(57) Linden, A. H.; Lange, S.; Franks, W. T.; Akbey, U.; Specker, E.; van Rossum, B. J.; Oschkinat, H. *J. Am. Chem. Soc.* **2011**, *133*, 19266−19269.
(58) Mak-Jurkauskas, M. L.; Bajaj, V. S.; Hornstein, M. K.; Belenky, M.; Griffin, R. G.; Herzfeld, J. *Proc. Natl. Acad. Sci. U. S. A.* **2008**, *105*, 883−888.
(59) Hu, F. H.; Luo, W. B.; Hong, M. *Science* **2010**, *330*, 505−508.
(60) Nieuwkoop, A. J.; Rienstra, C. M. *J. Am. Chem. Soc.* **2010**, *132*, 7570−7571.
(61) McAllister, R. G.; Konermann, L. *Biochemistry* **2015**, *54*, 2683−2692.
(62) Savage, D. F.; Egea, P. F.; Robles-Colmenares, Y.; O'Connell, J. D., III; Stroud, R. M. *PLoS Biol.* **2003**, *1*, 334−340.
(63) Zhu, F. Q.; Tajkhorshid, E.; Schulten, K. *FEBS Lett.* **2001**, *504*, 212−218.
(64) Wang, Y.; Tajkhorshid, E. *J. Nutr.* **2007**, *137*, 1509s−1515s.
(65) Ho, B. K.; Gruswitz, F. *BMC Struct. Biol.* **2008**, *8*, 49−54.

DOI: 10.1021/jacs.8b03446
J. Am. Chem. Soc. 2018, 140, 7885−7895